Toward an Astrophysical Theory of Chondrites

Frank H. Shu; Hsien Shang; Typhoon Lee

Science, New Series, Volume 271, Issue 5255 (Mar. 15, 1996), 1545-1552.

Toward an Astrophysical Theory of Chondrites

Frank H. Shu,* Hsien Shang, Typhoon Lee

The chondrules, calcium-aluminum–rich inclusions (CAIs), and rims in chondritic meteorites could be formed when solid bodies are lifted by the aerodynamic drag of a magnetocentrifugally driven wind out of the relative cool of a shaded disk close to the star into the heat of direct sunlight. For reasonable self-consistent parameters of the bipolar outflow, the base and peak temperatures reached by solid bodies resemble those needed to melt CAIs and chondrules. The process also yields a natural sorting mechanism that explains the size distribution of CAIs and chondrules, as well as their fine-grained and coarse-grained rims. After reentry at great distances from the original launch radius, the CAIs, chondrules, and their rims would be compacted with the ambient nebular dust comprising the matrices, forming the observed chondritic bodies.

The primary repository of information concerning the early history of solids in our own solar system resides in the meteorites, of which the chondrites form the most common and most unaltered examples (*1*). Chondrites are named after the quasi-spherical, once-molten, millimeter-sized features embedded within their matrices known as chondrules. Chondrites are important astrophysically because (i) they define the age of the solar system (4.56 billion years, with a spread of 10^7 years at most for the time of solidification of their inclusions), (ii) of all the meteorites, they most resemble the sun in their composition of condensable heavy elements, and (iii) they represent the first steps in the process by which nebular dust is transformed into the planets of the inner solar system (*2–4*). Chondrites as a whole were evidently assembled from the solids of the nebular disk from which the sun itself accreted 4.56 billion years ago. Consistent with the astronomical evidence on young stellar objects, these processes probably lasted only a few million years (*5*).

The component parts of chondrites—chondrules, calcium-aluminum–rich inclusions (CAIs), and their associated rims—and the chemical and mineralogical relations that these structures bear to the matrix material present enigmatic puzzles for astrophysical models of the early solar nebula (*6*). We may state the conundrum simply. The parent bodies of chondritic meteorites originate about 2.5 astronomical units (AU) from the sun, near the 3:1 resonance with Jupiter that throws collision fragments of asteroids into Earth-crossing orbits (*7*). On the other hand, the components of such meteorites show evidence of having undergone transient episodes of heating, lasting from an hour or less for chondrules to tens or hundreds of hours for CAIs (*8, 9*). Peak temperatures reached roughly 1500 to 2200 K, sufficient to melt these objects and vaporize some of their constituents. Temperatures in excess of a few hundred kelvin and heating or cooling times shorter than decades characterize no conventional model of the solar nebula at a distance of 2.5 AU from the primitive sun, neither from theory (*10*) nor from radio-interferometric observations most sensitive to the temperature of submillimeter- to centimeter-sized objects in the disks around young sunlike stars (*11*).

Chondrules occupy more than half of the volume of many common chondrites (*1*). Conservatively, 50% by mass of all the magnesium-iron silicates that went into planetesimals and planets experienced chondrule-forming events (*4*). A mass greater by a factor of about 100 could be involved if the rest of the rocky solids originally present in the solar system suffered a similar fate before being accreted by the sun. The mass-fraction of CAIs is smaller than that of chondrules by a factor of about 20; nevertheless, CAIs include a major part of the most refractory of the rock-bearing material in meteorites [principally calcium-aluminum oxides and silicates with melting temperatures ~1800 K and vaporization temperatures ≳2000 K (*4*)]. Thus, the formation of chondrules and CAIs must constitute a common outcome of the processes that solids undergo in nebular disk evolution.

Many hypotheses, such as collisions, lightning, flares, and shocks, have been advanced to explain the extreme thermal events experienced by chondrites (*4*). None have gained general acceptance (*12*). We adhere to the view that CAIs, chondrules, and their rims originated at a distance of about 0.06 AU ($\approx 13 R_\odot$, where $R_\odot$ is the radius of the sun) and were thrown out to planetary distances, where they aggregated with the ambient dust to form larger chondritic bodies (*13, 14*). The driver for the process was a bipolar outflow characteristic of the most violent stages in the formation of a sunlike star (*15*).

Magnetocentrifugally driven winds and funnel flows. A detailed quantitative model has recently appeared for bipolar outflows from and funnel flows onto newborn magnetized stars (*16–19*). In this model (Fig. 1), an accretion disk interacts with the rotating magnetosphere of a young star with the ideal unperturbed form of a pure dipole. If the star has mass M_*, radius R_*, and magnetic dipole moment μ_*, and if the disk mass accretion rate is $\dot{M}_D$, then the disk is truncated at an inner radius (*20*)

$$R_x = \Phi_{dx}^{-4/7} \left(\frac{\mu_*^4}{G M_* \dot{M}_D^2} \right)^{1/7} \qquad (1)$$

where G is the universal gravitational constant and Φ_{dx} is a dimensionless coefficient. The disk inflow at rate $\dot{M}_D$ divides at R_x into a wind outflow (known as the x-wind) at rate $\dot{M}_w = f\dot{M}_D$ and a funnel inflow onto the star at rate $\dot{M}_* = (1 - f)\dot{M}_D$. In the model preferred by (*18, 19*), $\Phi_{dx} \approx 1$ and $f \approx \frac{1}{3}$. In steady state, the stellar spin rate corotates with the inner disk edge

$$\Omega_* = \left(\frac{G M_*}{R_x^3} \right)^{1/2} \qquad (2)$$

The formation of a sunlike star surrounded by a planetary system occupies five schematic stages [see figure 7 of (*15*)]. A bipolar outflow is present in the third and fourth stages, when the central star is still embedded in its natal infalling envelope of gas and dust and when the outflowing wind has reversed the infall over almost all solid angles and revealed the central star and sur-

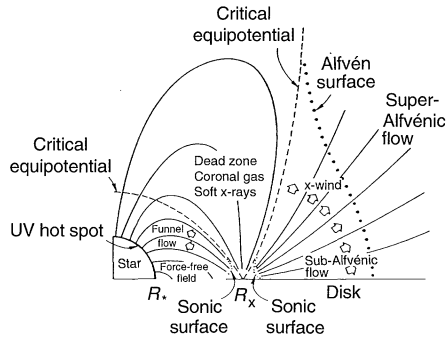

Fig. 1. Schematic diagram of the interaction of a magnetized star and a surrounding accretion disk. [Reprinted from (*16*)]

F. H. Shu and H. Shang are in the Astronomy Department, University of California, Berkeley, CA 94720–3411, USA. T. Lee is with the Institute of Earth Science, Academia Sinica, Taipei 115, Taiwan.

*To whom correspondence should be addressed.

rounding accretion disk as optical and near-infrared objects. Parameters typical of the embedded phase are $M_* = 0.5M_\odot$, $R_* = 3R_\odot$, $\mu_* = 2 \times 10^{37}$ G cm^3 (corresponding to $B_* \approx 2 \times 10^3$ G), and $\dot{M}_D = 1 \times 10^{20}$ g s^{-1} ($\approx 2 \times 10^{-6}$ $M_\odot$ year^{-1}). With these values, we get $R_x = 12R_\odot = 4R_*$, $\dot{M}_w = 3 \times 10^{19}$ g s^{-1}, and $2\pi/\Omega_* = 6.8$ days. For the revealed phase, we might have $M_* = 0.8M_\odot$, $R_* = 3R_\odot$, $\mu_* = 1 \times 10^{37}$ G cm^3 (corresponding to $B_* \approx 1 \times 10^3$ G), and $\dot{M}_D = 6 \times 10^{18}$ g s^{-1} ($\approx 1 \times 10^{-7}$ $M_\odot$ year^{-1}). In this case, $R_x = 16R_\odot = 5.3R_*$, $\dot{M}_w = 2 \times 10^{18}$ g s^{-1}, and $2\pi/\Omega_* = 8.3$ days. The last value corresponds well with the typical spin period of T Tauri stars (*21*). With a stellar mass accretion rate $\dot{M}_* = (2/3)\dot{M}_D$, it takes about 2×10^5 years to build the $0.5M_\odot$ star to a $0.8M_\odot$ star, and another 3×10^6 years to get from the $0.8M_\odot$ star to a $1.0M_\odot$ star, in rough agreement with the empirical lifetimes of the embedded and revealed stages.

Gas-solid coupling and aerodynamic size-sorting. Small, solid bodies can be carried out of the disk by the outflowing wind. The calculations are most efficiently computed in dimensionless form where

$$R_x,\ \Omega_*^{-1} \text{ and } \frac{\dot{M}_w}{4\pi R_x^3 \Omega_*} \qquad (3)$$

are the units of length, time, and density (*16*, *17*). For a spherical protochondrule or protoCAI of radius R_c and internal density ρ_c, the relevant aerodynamic coupling constant is

$$\alpha \equiv \frac{3C_D\dot{M}_w}{16\pi\Omega_* R_x^2 \rho_c R_c} \qquad (4)$$

where C_D is the drag coefficient (a dimensionless number of order unity).

Small particles with $\alpha \gg 1$ are well coupled to the gas and will be thrown into interstellar space with finite escape speeds, whereas large particles with $\alpha \ll 1$ decouple early from the x-wind and fall back to the disk at a reentry radius not much bigger than R_x. Particles corresponding to $\alpha \approx 0.4$ and starting in the middle of the x-wind are thrown to great, but not infinite, distances before reentering the disk (Fig. 2). Particles of the same size or larger (the same α or smaller) will fall out of the flow close to the launch radius R_x if they are initially lifted by the weaker parts of the outflow. They will then be carried back to the x-region as part of the general disk accretion process, where they have a one-third chance of attaching onto another wind streamline that carries them away from the star and a two-third chance of being lifted by a funnel streamline that carries them into the star.

Particles that suffer sufficient radiative heating by being lifted from the disk, where they are shaded from the starlight, and that land near 2.5 AU are candidates for the chondrules and CAIs found in chondritic meteorites. Our model predicts that chondrules and CAIs should be sprayed over the entire solar system and should be found among sufficiently primitive solid materials at all distances from the sun. Thus, comets should also contain CAIs and chondrules. With $\alpha = 0.4$ for the median streamline at any epoch, $C_D = 1$, and $\rho_c = 3$ g cm^{-3}, the process in the two fiducial epochs aerodynamically sorts for objects of diameters $2R_c$, equal to 3 mm and 0.2 mm. Combined with variations of a factor of 2 about the median streamline, the x-wind naturally sorts for rocks of the observed range of sizes of CAIs and chondrules.

The base temperature. An optically thick, purely absorptive, completely flattened portion of a disk lying at a distance R_x exposed to the oblique rays from a central star of radius R_* and luminosity L_* has a reprocessing temperature given by (*22*)

$$T_x = \left\{ \frac{L_*}{4\pi^2\sigma R_*^2} \left[\arcsin\left(\frac{R_*}{R_x}\right) - \left(\frac{R_*}{R_x}\right)\left(1 - \frac{R_*^2}{R_x^2}\right)^{1/2} \right] \right\}^{1/4} \qquad (5)$$

where σ is the Stefan-Boltzmann constant. In deriving Eq. 5, we assumed that the contribution from viscous heating is zero at the inner disk edge.

The stellar luminosity L_* during the embedded phase arises mostly from the accretion luminosity released by the funnel flow as it impacts the star at hot spots located at a mean colatitude θ_h (*19*)

$$L_{hot} = (1 - f)\frac{GM_*\dot{M}_D}{R_*}\left(1 + \frac{R_*^3}{2R_x^3}\sin^2\theta_h - \frac{3R_*}{2R_x}\right) \qquad (6)$$

For the preferred model, $\sin\theta_h \approx 0.5$ when $R_*/R_x = 1/4$. Together with the other fiducial parameters, we then have $L_{hot} = 3.6L_\odot$. To this accretion luminosity we need to add the nuclear luminosity of steady-state deuterium burning (*23*), which amounts to about $0.8L_\odot$ in the present case if we adopt a D/H abundance (in mass) of 2×10^{-5}. Thus, the self-consistent stellar luminosity $L_* = 4.4L_\odot$.

The luminosities of T Tauri stars arise mostly from gravitational contraction at a nearly fixed surface temperature T_*. With $T_* = 4000$ K for the fiducial revealed source, the resulting stellar luminosity is $4\pi R_*^2\sigma T_*^4 = 2L_\odot$. Making a correction for accretion and deuterium burning, we adopt $L_* = 2.5L_\odot$.

Equation 5 now implies that temperatures at the base are $T_x \approx 1200$ and 800 K, respectively, for the embedded and revealed examples. These temperatures give the starting value for the solids before they are launched by the wind and may be too hot for the partial retention of moderately volatile elements by chondrules (*24*, *25*). An upper limit of 650 K for the precursors to chondrules has been argued from the evidence on FeS (*26*), but sulfide and metal in chondrules may also be metamorphic in origin (*12*). If so, upper limits to the base temperature closer to 1000 K, from the retention of Na and K, would be more realistic.

The surface-averaged temperature of a launched particle. The surface-averaged temperature of a launched particle with size appreciably larger than the wavelength of

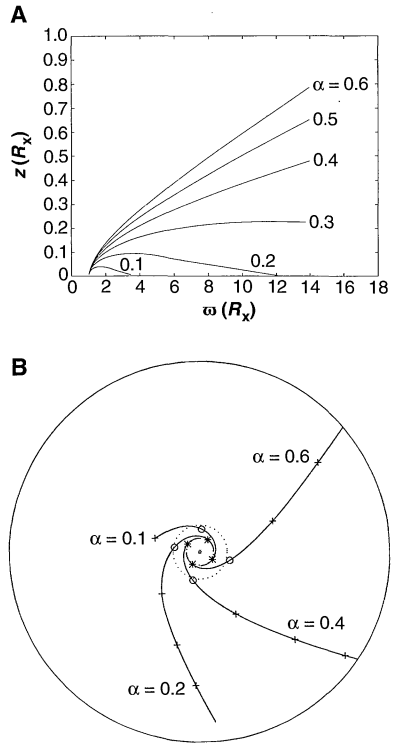

Fig. 2. (**A**) Meridional-plane view of the trajectories followed by particles with gas-drag coupling constant $\alpha = 0.1$, 0.2, 0.3, 0.4, 0.5, and 0.6. The unit of length is R_x; z and ϖ are cylindrical coordinates. The vertical scale is stretched with respect to the horizontal scale, so that the particles fly on trajectories considerably flatter than the gas streamlines depicted in Fig. 1. (**B**) Equatorial projection of the trajectories followed by particles in an inertial frame with $\alpha = 0.1$, 0.2, 0.4, and 0.6. The trajectories are spirals because the x-wind, especially in its inner part, rotates as well as blows outward. Notice that the cases $\alpha = 0.1$ and 0.2 impact the disk before reaching the outermost circle of radius $14R_x$. The trajectories begin just slightly outside R_x (the inner dotted circle; the outer dotted circle is $2R_x$), and the symbols mark the passage of time after 1, 4, 10, 20, and 30 units of Ω_*^{-1}.

the light that it emits or absorbs can be estimated from the general radiation-equilibrium condition

$$\overline{T}_{eq} = T_L\left[\frac{\mathcal{F}_{D*}}{r^2}\exp(-\tau_*) + \frac{\mathcal{E}}{aT_L^4} + C_w\rho w^3\right]^{1/4} \quad (7)$$

with

$$T_L \equiv \left(\frac{L_*}{16\pi\sigma R_x^2}\right)^{1/4}, \quad C_w \equiv \frac{\dot{M}_w\Omega_*^2R_x^2}{2L_*} \quad (8)$$

In Eq. 7, $\mathcal{F}_{D*} \leq 1$ is the reduction factor resulting from partial occultation of the star by a disk with a central hole in it; τ_* is a representative optical depth for unocculted starlight from the protosun to the particle located at a dimensionless radius $r \equiv R/R_x \geq 1$; $\mathcal{E}$ is the dimensional energy density of the diffuse radiation field at this position in the flow; a is the radiation constant; and the term $C_w\rho w^3$ is the ratio of the equivalent spherical rate of aerodynamic heating per unit area—$\rho w^3/8$ in dimensionless form, times its scale factor $\dot{M}_w\Omega_*^2/4\pi$—to the unshielded surface-average of the radiative heat input $L_*/16\pi R_x^2$ at R_x.

When a solid particle is inside an optically thick disk, τ_* is essentially infinite, ρw^3 is essentially zero, the diffuse radiation field is given by $\mathcal{E} = aT_x^4$, and Eq. 7 recovers the equilibrium temperature as the base value $\overline{T}_{eq} = T_x$. Gently lifting this particle into the wind (where τ_* is zero, or at least not large) will heat the particle dramatically. For $r = 1$ ($R = R_x$), $\tau_* = 0$, $\mathcal{F}_{D*} = 1$, $\mathcal{E} = aT_x^4/2$ (the diffuse radiation field approximated as half of a blackbody from the underlying disk), and negligible aerodynamic heating, the particle acquires a surface-averaged peak temperature of

$$\overline{T}_{peak} = \left(T_L^4 + \frac{1}{2}T_x^4\right)^{1/4} \quad (9)$$

The approximation of negligible aerodynamic heating yields a good estimate for the peak temperature, because $C_w = 0.07$ in the embedded phase (smaller in the revealed case) and ρw^3 is nowhere larger than ~0.1 (Fig. 3).

For the fiducial embedded and revealed cases, $\overline{T}_{peak} = 1800$ and 1300 K, respectively, with most of the contribution coming from direct sunlight T_L. The first value is sufficient to melt most rocky materials; the second is somewhat too low. If we take the results literally, we would expect CAIs to form in the embedded phase and chondrules in an epoch that may include both embedded and revealed phases. However, fractal assemblages (*27*) may reach higher subsolar temperatures than melted spherical droplets.

Fractal heating and conductive cooling. For a solid or molten sphere of rock ~1 mm in diameter, the radiative time to heat to or cool from ~1700 K is about the same, coincidentally, as the time to conduct the heat deposited at the surface into the interior: ~1 s. The averaging in Eq. 8 of the heat deposited onto the cross-sectional area πR_c^2 over $4\pi R_c^2$ of total surface area is therefore only valid for formed CAIs or chondrules that spin with periods shorter than 1 s and have their rotation axis changed randomly on time scales rapid compared with 1 s (otherwise, equator-to-pole variations will still occur). Spin periods shorter than 1 s can indeed be expected for CAIs or chondrules if they are bombarded by numerous dust particles flying differentially through the wind. Reorientation of the direction of the spin axis by an occasional large hit, however, may take many minutes to hours.

Empirically, the most extreme flattening reported for chondrules in chondritic meteorites is an axial ratio of 2.36:1 (*28*), close to the critical value 2.48:1 computed by Chandrasekhar for the onset of fission instability in a rotating liquid drop whose shape is maintained by surface tension (*29*). With an estimate of 500 erg cm^{-2} for the surface tension of molten rock, the corresponding spin period for a droplet of diameter $2R_c = 1$ mm is 2 ms. Intact chondrules as aspherical as the critical state are rare; thus, most chondrules must have possessed spin periods longer than 2 ms when they solidified from a molten state.

Moreover, protoCAIs and protochondrules are unlikely to start with the internal density or thermal conductivity of compacted rock. Inside a turbulent disk, dust grains probably form fluffy aggregates reminiscent of cometary or interplanetary dust particles (*30*). Interlocking of aggregates through their many open branches (*14*) or through van der Waals bonding may produce dustballs up to a few centimeters in size (*31*).

Exposure to direct sunlight can heat the dustballs sufficiently to melt the solids and close the open spaces, creating CAIs and chondrules. Aerodynamic sorting by the outflowing bipolar wind then ejects the smallest bodies to interstellar space, whereas the largest ones fall out of the flow back onto the disk.

For the same mass and angular momentum, dustballs tumble slower than their compact molten counterparts, and they also have lower effective conductivities and longer conduction times (*32*). If the spin period and conduction time become longer than the radiation deposition time, the temperature at the subsolar point could exceed the value calculated by Eq. 9 by as much as a factor of $\sqrt{2}$. Subjected to direct sunlight, then, a dustball with a mean surface temperature $\overline{T}_{peak}$ that is too low can still melt at its near-subsolar positions, with the liquid collecting gradually in a spherical pool as the dustball turns in space. The compact sphere cools to a temperature close to $\overline{T}_{peak}$ because it can conduct its radiatively deposited heat to the interior and night side of the particle on a time scale of ~1 s. The sphere continues to grow in mass until appreciable differential motions develop between it and the fractal superstructure (until α for the sphere decreases to a number of order unity). For a dustball superstructure with mass comparable to the final chondrule formed, the process occupies the many minutes that it takes to reorient randomly the spin axis of the dustball. The dustball therefore retains an open structure only during the relatively short interval when even a compact sphere of the same mass would be well coupled to the surrounding dense wind; thus, we are justified in making trajectory calculations that ignore the fractal structure of the initial assemblage.

Instability of the liquid phase. The x-wind model shares a difficulty in common with other mechanisms for producing melts in the early solar system: too low a partial pressure of the corresponding vapor for thermodynamic stability of the liquid phase. This deficiency has the consequence that molten droplets tend to evaporate. We simplify the discussion by using a single component to describe what is in reality a complex mix of chondrule or CAI compositions. Exchange with the gas phase modifies the mass of a molten droplet at the net rate (*33*)

$$4\pi\rho_c R_c^2\frac{dR_c}{dt} = 4\pi R_c^2[P_m - P_v(T)]\left(\frac{2\pi kT}{m}\right)^{-1/2} \quad (10)$$

where P_m is the partial pressure of the substance molecules of mass m, $P_v(T)$ is the

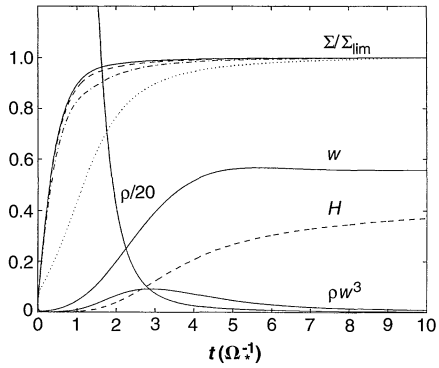

Fig. 3. The dimensionless gas density ρ (divided by 20), relative velocity w, and drag heating term ρw^3 experienced as a function of orbit time by a particle launched on the median streamline. Also displayed are the cumulative integrals Σ and H (Eqs. 12 and 14), with the former normalized with respect to its limiting value Σ_{lim} at large t. Normalized curves Σ/Σ_{lim} are displayed for $v_t = 0$ (dotted curve), $v_t = \varepsilon$ (dashed-dotted curve), $v_t = 2\varepsilon$ (dashed curve), and $v_t = 3\varepsilon$ (solid curve), where $\varepsilon = 0.03$ is the dimensionless isothermal sound speed. The limiting value Σ_{lim} equals 13.5, 46.9, 88.2, and 130 for these four cases, respectively.

saturation vapor pressure, and k is Boltzmann's constant. We have assumed unit accommodation of the incident gas molecules by the liquid surface and ignored slight corrections to the vapor pressure arising from the effects of surface tension in a droplet of finite size. At $T \approx 1700$ K for a typical silicate melt, $P_v(T) \approx 1$ dyne cm^{-2} (*34*). The available partial pressure P_m in an x-wind is negligible in comparison with the latter value for $P_v(T)$; therefore, the time to completely evaporate a molten droplet of initial radius R_c under conditions of constant ρ_c and T is

$$t_{evap} = \frac{\rho_c R_c}{P_v(T)} \left(\frac{2\pi kT}{m}\right)^{1/2} \quad (11)$$

With the previously cited values for T and $P_v(T)$ and $m \approx 10^2$ atomic mass units, the time to evaporation $t_{evap} \sim 3$ hours for a particle of diameter $2R_c = 1$ mm.

Thus, in order for chondrules to survive the melting process and not evaporate away completely, they must not be kept above the melting temperature much in excess of 3 hours, a result consistent with the cooling time scales deduced from chondrule textures. If chondrules reach true peak temperatures substantially higher than 1700 K, the required cooling time may become as short as tens of minutes (*35, 36*), which can be accommodated by our mechanism of fractal melting followed by conductive cooling to values of $\overline{T}_{peak}$ below 1700 K. Molten CAI droplets can presumably survive evaporative losses despite the longer time scales (days) to which they are exposed to high temperatures because they are often physically bigger and the vapor pressures of calcium-aluminum oxides and silicates are much lower than those of magnesium-iron silicates at the same temperatures.

The formation of CAIs. An unshielded, radiatively heated body declines in surface-averaged temperature from a peak $\overline{T}_{peak}$ on the liquidus to values below it on roughly the time scale Δt required for the particle to increase its original orbital radius to about $1.5R_x$. Figure 2B shows that $\Delta t \approx 2\Omega_*^{-1}$, which equals about 50 hours for the fiducial embedded case.

Only the most refractory inclusions (CAIs) can withstand an impulsive rise to temperatures higher than 1800 K (by the fractal heating mechanism) followed by an extended treatment for many hours at $\overline{T}_{peak} \approx 1800$ K. Such materials constitute by mass ~5% of the total original rocky material and do not contain enough optical depth to provide appreciable mutual shading. Thus, the approximation of unshielded test particles, with a characteristic time scale $\sim 2\Omega_*^{-1}$ for mean exposure to full sunlight, is a reasonable assumption for CAIs, if they are formed in the embedded phase of protostellar evolution.

The condensation of CAI rims. The fine-grained rims of CAIs form a good test of the above picture. The less refractory silicates that evaporate upon launch from R_x recondense from the vapor phase as the wind expands and cools appreciably below a temperature of ~1700 K. The intact CAIs constitute good condensation nuclei for this process and acquire rims with the chemical composition of the vaporized material. Observed CAI rims often display layers that have sequentially lower condensation temperatures as one moves radially outward from the center of the CAI (*9*).

We can quantitatively test the model by calculating the mass of condensable solids swept up by a CAI as it flies through the x-wind. The dimensionless mass of gas encountered per unit cross-sectional area of a body during its flight is

$$\Sigma = \int_0^t \rho \, \sup(w, v_t) dt \quad (12)$$

where ρ and v_t are the dimensionless gas density and turbulent velocity (perhaps zero) in the wind and $\sup(w, v_t)$ is the larger of w and v_t (Fig. 3) (when $w < v_t$, the effective speed at which individual molecules encounter the body is the turbulent velocity v_t; when $w > v_t$, the effective speed is the relative flow velocity w).

For simplicity, we assume that molecules are efficiently implanted in the growing rim independent of the relative velocity of gas and solid and that refractory elements remain bound to the surface as long as the solid lies below the condensation temperature of the corresponding material. The appropriate $\Delta\Sigma$ to use from Fig. 3 is then the difference between the asymptotic value of Σ at large times and its value when $\overline{T}_{eq}$ in Eq. 7 drops below ~1700 K. To obtain the mass ΔM of deposited rim material, we have to multiply this value of $\Delta\Sigma$ by the product of (i) χ_{si}, the mass fraction of silicate-like materials in a cosmic mixture, (ii) πR_c^2, the cross-sectional area of a (tumbling) CAI over which condensation occurs, and (iii) $\dot{M}_w/4\pi R_x^2\Omega_*$, the dimensional unit of surface density (the product of the first and third quantities in Eq. 3). If we approximate the density of the rim material as the internal density of the CAI, then the rim thickness ΔR compared to the CAI radius R_c is given (for a thin rim) by

$$\frac{\Delta R_{fine}}{R_c} = \frac{\chi_{si}\dot{M}_w\Delta\Sigma}{16\pi\Omega_* R_x^2 \rho_c R_c} = \frac{\chi_{si}\alpha\Delta\Sigma}{3C_D} \quad (13)$$

where we have used Eq. 4 to derive the last equality. With $\chi_{si} = 0.4\%$, $C_D = 1$, and $\alpha = 0.4$, we need $\Delta\Sigma = 80$ to 160 to get agreement with the measured thicknesses of CAI rims, $\Delta R_{fine}/2R_c \approx 2$ to 4% (*9*). If condensation of silicates begins immediately after launch, we infer turbulent velocities in the x-wind about three times the isothermal sound speed, $v_t \approx 3\varepsilon$. Supersonic but sub-Alfvénic turbulence is possible for the magnetized x-wind, especially the part that rubs against the surface of the disk. Extremely thick examples of fine-grained rims may require multiple coatings, that is, several aborted launches followed by a successful boost to planetary distances.

The formation of chondrules and their rims. Chondrules are probably formed during a later phase (embedded or revealed) when the base and surface-averaged peak temperatures, T_x and $\overline{T}_{peak}$, are lower than those for CAIs. If $1700 \text{ K} > \overline{T}_{peak} > 1300$ K (which implies even higher subsolar temperatures for fractally heated dustballs), the temperatures will be enough to vaporize moderately volatile substances on a time scale short compared to an hour but not enough to vaporize silicate rocks.

For evidence in support of the above picture, we again look to the rims. Chondrules have two types of rims: coarse-grained and fine-grained, with the latter sometimes overlaid on the former (*35*). The first type of rims contains coarse grains roughly 10 μm in diameter with devolatilized compositions that are chemically similar to the body of the chondrule. The second type contains fine grains of submicrometer sizes with volatile-rich compositions that are chemically similar to the matrix material of chondrites.

Coarse-grained rims may form by collision of the slower moving, tumbling, now solidified chondrules with faster moving, better coupled dust or dustballs. Equation 13 implies that the mass of impacting dust makes only a small contribution to the thicknesses of coarse-grained rims (although occasional slow collisions between two plastic bodies of similar size can lead to a compound chondrule); more important is the remelting of the chondrule mantle by the energy of the collision followed by local recrystallization. Because small dust grains and dustballs have almost the same velocity relative to chondrules as the gas, the cumulative energy deposited per unit area into the mantle is proportional to

$$H \equiv \int_0^t \rho w^3 dt \quad (14)$$

times the mass fraction χ_{si} contained in silicate grains (Fig. 3).

Adopting melt yields that are proportional to the kinetic energy of the impactor and assuming that the relevant formation interval corresponds to the difference integral ΔH, we obtain coarse-grained rims of fractional thicknesses (see the derivation of Eq. 13)

$$\frac{\Delta R_{course}}{R_c} = Y_f \left(\frac{R_x \Omega_*}{v_f}\right)^2 \left(\frac{X_{si} \alpha \Delta H}{3 C_D}\right) \quad (15)$$

where $Y_f = 6$ is the melt mass as a multiple of the impactor mass at the fiducial impact velocity $v_f = 7.44$ km s^{-1} [see equation 3.1 and figure 8b in (*37*)]. The maximum ΔH possible is the asymptotic value ~0.4 reached by H in Fig. 3. For $C_D = 1$, $X_{si} = 0.4\%$, and $\alpha = 0.4$, we then get $\Delta R_{coarse}/2R_c \approx 10\%$ during both the embedded and revealed phases. This value is somewhat less than the measured fractional thicknesses of coarse-grained rims surrounding ordinary and CV3 chondrites, $\Delta R_{coarse}/2R_c \approx 15$ to 40% (*35*). Given the uncertainties, the discrepancy is not worrisome. For example, there may be an enhancement of the rock-to-gas ratio X_{si} above the conventional value, either locally because of inhomogeneities in a turbulent disk (*38*) or globally because of the recycling of solids back to the disk by means of the x-wind.

Fine-grained rims may form from less refractory rocky material that vaporized when nebular solids were first lifted out of the disk by the x-wind. The fine-grained rims would then condense on the nucleation centers of the protochondrules when the wind expands and cools. Such condensation products should have submicrometer sizes, an empirically known result for dust that condenses from red-giant winds (*39*).

Time for cooling of molten chondrules. Computations of the temperature history of solids are sensitive to the assumed size distribution of particles that contribute to the optical depth τ_* in Eq. 7. If small silicate grains survive evaporation, dustballs launched on a restricted subset of streamlines near the uppermost one can produce chondrules. Because of their flat trajectories (Fig. 2A), molten bodies of the appropriate size move quickly into the shade provided by the small dust grains entrained in the upwelling gas of the bipolar outflow. When the optical depth associated with the dust is appreciable, such molten bodies can cool down much more quickly than if they were to remain fully exposed to the light of the sun.

In the revealed stage, the wind does not contain enough dust to make it optically thick (otherwise the central star would not be revealed as an optical object). The discussion then simplifies considerably. No object launched in this stage on any streamline can reach surface-averaged peak temperatures great enough to melt silicate rocks. Fractal heating of dustballs may provide effective melting conditions for only tens of minutes, beyond which the compact protochondrule is cooled radiatively and conductively from $\overline{T}_{peak} \sim 1300$ K to much lower values on a time scale of days. Because all streamlines carrying dustballs can experience this form of chondrule making, the efficiency of the process is high during the revealed phase of protostellar evolution. The chondrules formed are small, and because of the relative lack of small impacting grains (most of the dustballs having been converted to protochondrules), they acquire only thin coarse-grained rims that are easily destroyed when these objects reenter the disk.

Consistent with this picture, the chondrules in CO3 meteorites (the least metamorphosed of the CO group) have mean sizes of 0.15 mm (*40*), and only ~1% of them possess coarse-grained rims (*35*). In contrast, the chondrules in CV3 meteorites have mean sizes of 1.0 mm (*41*), and ~50% of them possess coarse-grained rims (*35*).

An extended period (days) of temperatures above 1000 K, implied by either of the mechanisms for producing chondrules, seemingly contradicts the evidence concerning the partial retention of Na in these objects (*8*, *12*, *26*). The retention of volatile Na in chondrules is aided by high oxygen fugacity (*42*). High oxygen fugacity also appears necessary to explain the enhanced loss from CAIs of W and Mo, whose oxides evaporate much more readily than their highly refractory metallic states (*43*). The condition of high oxygen fugacity likely applies in the x-wind because the ultraviolet light from the hot spot can photodissociate H_2O, liberating oxygen even in the relatively abundant presence of hydrogen. If H_2O is totally dissociated, the partial pressure of O exceeds 3×10^{-10} atm for dimensionless time $t < 1.5$ (where temperatures near the peak values are reached) in the fiducial embedded case. The corresponding oxygen fugacity would allow considerable Na retention under experimental conditions that reproduce likely chondrule-formation thermal histories (*42*). Astronomically, it is known from [O I] emission at 6300 Å that free atomic oxygen is present in T Tauri winds at a distance of ~10 to 100 AU (*44*).

The efficiency of the formation of CAIs and chondrules. For every 3 g of material brought through the disk, 1 g is processed through an x-wind, and 2 g are dumped onto the protosun by the funnel flow. In other words, to make a $1M_\odot$ star from a $0.8M_\odot$ revealed source requires $0.1M_\odot$ of gas to be blown out by the x-wind. Even if only 13% of the silicate dustballs associated with this amount of gas is in the right size range to be processed into molten droplets that eventually fall back into the disk, the total mass of chondrules produced equals that of all of the rock contained in the planets of the solar system (*45*).

The CAIs form by the same basic mechanism as chondrules, except that the conditions required to form CAIs are met only during the embedded stage of protostellar evolution, and the raw material to make them constitutes only 5% of the total. Indeed, CAIs occupy volume fractions of 6 to 12%, 10 to 15%, and 5%, respectively, in the CV, CO, and CM chondrites, and only <1% and ≪1%, respectively, in the ordinary and enstatite chondrites (*35*). This trend is accompanied by (i) a decrease in the mean chondrule size, from ~1 to ~0.2 mm, (ii) a decrease in the percentage of chondrules with coarse-grained rims, from 50 to <1%, and (iii) an increase in abundance of the more volatile metal and sulfide species as we progress from the CV to CO and CM carbonaceous chondrites, and from the LL, L, and H ordinary chondrites to the EL and EH enstatite chondrites (35). However, carbonaceous and ordinary plus enstatite chondrites seem to form two separate sequences in their properties. In distinguishing carbonaceous chondrites from ordinary ones, greater original distance from the protosun for assemblage of the whole body may play an additional role to a generally earlier time of origin.

The matrices of chondrites. The pristine matrix material of chondrites probably never occupied a spatial location very much inward of 2.5 AU. Apart from the brecciation, thermal metamorphism, and aqueous alteration that may have occurred after their incorporation into larger bodies, this matrix material is essentially compacted nebular dust (*46*).

Reentry of ejected CAIs and chondrules into the disk introduces a complication. Reentering objects experience high-speed collisions with ambient dust grains that ablate chondrule and rim material, adding the debris to the pristine matrix material. Conventional yield estimates (*37*) allow us to ignore the effects of gas sputtering in the destruction of the mantles of chondrules and CAIs. Further simplification is possible by ignoring any curvature of the relative orbit and any forces other than gas drag. In a single spatial dimension, the equation of motion of a reentering CAI or chondrule is then

$$\frac{4\pi}{3} \rho_c R_c^3 \frac{dv}{dt} = -C_D \pi R_c^2 \rho_g v^2 \quad (16)$$

where ρ_g and v are the (dimensional) gas density in the disk and the relative velocity of the solid object (assumed in the equation of motion to have fixed mass) and the gas. When a small dust particle hits the CAI or chondrule, the particle excavates an amount of material proportional to its kinetic energy. If v_e is the speed at which the dust grain excavates its own mass (below which we consider no net losses to occur), the rate of mass loss is

$$4\pi \rho_c R_c^2 \frac{dR_c}{dt} = -\pi R_c^2 \left(\frac{v}{v_e}\right)^2 X_d \rho_g v \quad (17)$$

In Eq. 17, X_d is the mass fraction of dust, making the $X_d \rho_g v$ term the mass flux of dust grains of any type present in the nebular

disk (more than just silicates at distances greater than 2.5 AU).

Division of Eq. 17 by Eq. 16 yields an equation for dR_c/dv that is independent of the gas density history experienced by the CAI or chondrule in its reentry path into the disk if the column density of gas is much larger than the characteristic value $4\rho_c R_c/3$ required to slow down the CAI or chondrule by half. The integration of the equation for dR_c/dv from v equal to some initial value v_0 to a final (nondestructive) value v_e gives

$$\frac{R_c}{R_{c0}} = \exp\left[-\frac{\chi_d(v_0^2 - v_e^2)}{6C_D v_e^2}\right] \qquad (18)$$

where R_c and R_{c0} are, respectively, the final and initial radii of the reentering object.

For crystalline anorthosite, $v_e \approx 10$ km s^{-1} [see figure 8a in (*37*)]. We adopt somewhat arbitrarily $v_e = 5$ km s^{-1} for the weaker structures characteristic of the rims and outer mantles of chondrules. With $v_0 = 30$ km s^{-1}, we get an erosion of about 6% of the object's radius (or about 18% of its mass) for $\chi_d = 0.01$ and $C_D = 1$.

Thus, once CAIs and chondrules begin to reenter the disk in significant numbers, many small solid fragments of CAIs, chondrules, and their rims will be added to the ambient dust. Chondrites subsequently form with the matrix made from this eclectic mix of primitive nebular dust and processed fragments. Because fine-grained rims of chondrules occupy the most vulnerable outermost layers, they contribute disproportionally to the fragment population of the matrix mix. In chondrites where chondrules and their fragments dominate, this phenomenon leads to the interesting impression that chondrule material and matrix material are chemically complementary (*47*), because fine-grained rims are the recondensed evaporates of distilled chondrules.

Element fractionation among the chondrite classes. To explain the systematic fractionation patterns of two different groups of elements observed among the different chondritic groups, the refractory lithophiles (*48*) and the moderately volatile siderophiles (*25, 49*), Wood and others have developed an empirical mixing model. In our elaboration of this model, all pristine solid material in the solar nebula starts with the chemical composition of CI chondrites. Such chondrites have condensable element abundances virtually identical to the solar photosphere and possess neither CAIs nor chondrules. They are all that the solar nebula can produce during an initial fallow period, when $\dot{M}_D$ is so large in Eq. 1 that the characteristic temperature T_L in Eq. 8 exceeds the vaporization temperature of any form of solid, and neither CAIs nor chondrules are produced in the x-wind. As the x-wind develops the power to produce molten droplets of the most refractory solids and then gradually loses this ability, the disk gives birth to the carbonaceous sequence (CV, CO, and CM), with their varying abundance of refractory lithophile elements reflecting the addition of decreasing amounts of CAIs into the CI matrix material (Fig. 4). After the x-wind becomes inefficient at producing CAIs but while it still can make less refractory chondrules of successively smaller sizes, the disk yields in time the ordinary (LL, L, and H) and enstatite (EL and EH) chondrites. Because chondrules constitute a large fraction (up to 80%) of the volume of the ordinary and enstatite chondrites, the bulk compositions of these meteorites appear as if they had CI abundances minus the material associated with the CAIs and the related amoeboid olivine inclusions, which were blown out as small solid grains in the x-wind.

The depletion with respect to CI of moderately volatile siderophile elements in the other chondrites has a similar explanation, but now involving primarily the two components, chondrules and (pristine) matrix (*25, 49*). The loss of volatiles from chondrules and their fragments and the retention of this material by the matrix material largely explains the pattern of moderately volatile depletions seen in the carbonaceous and ordinary chondrites. Our elaboration of the mixing model resolves a mystery implicit in the original two-component formulation: why there exists no meteoritic class that is enriched in the moderate volatiles lost by the chondrites. The resolution is as follows. The same magnetohydrodynamic interaction of the protosun with the nebular disk that produces CAIs, chondrules, and rims in an x-wind also lifts the identical material in a funnel flow that feeds the protosun. Thus, the sun naturally acquires the same bulk composition of condensable heavy elements as CI chondrites. The totality of other chondrites have the same cosmic mix as the sun, except that they are missing the more volatile species, either left uncondensed in the wind or nucleated around small particles (which have most of the surface area) carried to interstellar space. This loss from the system then provides the reservoir for the overall volatile depletion seen in the chondrites.

The otherwise puzzling loss of both the most refractory and the most volatile substances from ordinary chondrites is a salient feature of the x-wind model. The effect arises from the mechanical selection for molten droplets. The most refractory parts of dustballs, whether intact or broken into individual grains, remain unmelted and well-coupled to the wind. They disappear from the solar system. The volatile parts of dustballs are vaporized and are also blown to interstellar space, unless they happen to recondense as a rim on a once-molten droplet with the correct size to fall back into the disk.

Chondrite chronology. According to the x-wind model, a difference of a few million years separates the main epochs of CAI and chondrule formation, although smaller differences might appear in CAIs and chondrules found in the same meteorite. Recent interpretations of the levels of the extinct nuclide ^{26}Al in CAIs and chondrules are consistent with this chronology (*50*). However, ^{26}Al may not be the perfect carrier of time information because (i) its radioactive-decay enrichment of ^{26}Mg over natural levels is readily detectable in CAIs (*51*) but not in protoplanetary chondrules (*50*) and, (ii) rather than providing clocks of earlier external seeding, ^{26}Al may be produced by cosmic-ray reactions inside the early solar system (*52*). The x-wind model lends credence to the latter idea because it may overcome the basic objection that insufficient cosmic-ray flux of protostellar origin impinges on target atomic nuclei at 2.5 AU when energetic particles associated with T Tauri flares are spread out over the entire surface area of the disk. In the x-wind model, flares may arise in reconnection events involving large magnetic loops that have one footpoint on the star and one in the x-region of the disk (Fig. 1) (*19*). En-

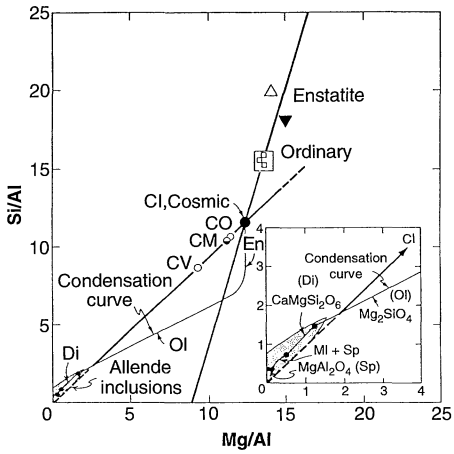

Fig. 4. The mixing diagram for aluminum, magnesium, and silicon. Cosmic ratios of these elements, as represented by the data point for CI chondrites, lie in the middle of this diagram. If carbonaceous chondrites had consisted entirely of CAIs (rich in Al but containing little Mg or Si), they would fall in the part of the diagram labeled Allende inclusions. The actual CO, CM, and CV chondrites lie along a mixing line that reflects an addition of 5 to 15% of CAIs by volume fraction into CI material. In contrast, the ordinary and enstatite chondrites lie on a mixing line that also passes through CI, but from the other side and with a different slope. To generate their compositions from CI requires a subtraction of the most refractory lithophile elements, including but not exclusively CAI-like material. [Reprinted with permission from (*48*)]

ergetic charged particles (perhaps stored in closed field lines as radiation belts around the protosun) capable of producing nuclear reactions would then be partially focused to the base of the flow from where CAIs and chondrules originate.

Cameron has noted that solids tend to drift radially relative to the gas in a rotating disk that is partially supported against the gravity of the central star by gas pressure. This inward drift sets uncomfortable limits on how long CAIs or chondrules can reside at planetary distances in the disk (*14*). Cameron interprets this constraint to imply that CAIs are somehow temporarily stored without continued radial drift until the formation of chondrules. As a variation on this possibility within the context of the x-wind mechanism, CAIs can be sprayed to such great distances from the sun that the time required for them to drift back to 2.5 AU may occupy 10^6 years or more. Moreover, even when CAIs drift to the inner edge of the disk, they only possess a ⅔ chance of being funneled into the sun. There still exists a ⅓ chance that they can be thrown back to planetary distances. The production rate of CAIs (and chondrules) by the x-wind mechanism is potentially so great, even with losses to the sun or to interstellar space, that these bodies can be recycled several times through the disk without encountering difficulties.

Remnant magnetism in chondrites. Many chondrules in chondrites exhibit paleomagnetism, consistent with an interpretation that they passed through regions where the magnetic field had an intensity on the order of 1 to 10 G when the magnetic minerals cooled below their Curie (or related transition) temperatures of several hundred kelvin (*53*). This phenomenon is a necessary consequence of the x-wind picture because the driving mechanism for the flow relies on the existence of strong magnetic fields. The characteristic unit of field strength that accompanies the choices of Eq. 3 is $(\dot{M}_w\Omega_*/R_x)^{1/2}$ (*16*, *17*), which equals 20 and 4 G for the two fiducial cases. At a distance of $10R_x$, where we can expect the particle temperature to have fallen to below 600 K, the field would have dropped to about 0.2 in the above units, or about 4 and 0.8 G for the embedded and revealed cases, respectively (Fig. 5).

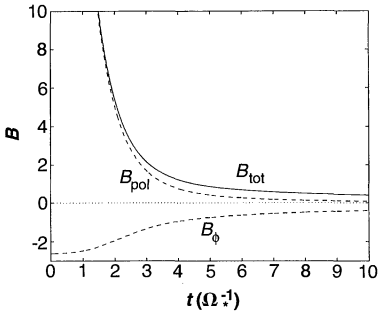

Fig. 5. The dimensionless magnetic field encountered as a function of orbit time by a particle launched on the median streamline. Close to the launch point, the primary contribution to the total field strength B_{tot} in the x-wind comes from the (trapped) poloidal contribution B_{pol}, but far from the star, it comes primarily from the (negative) toroidal contribution B_ϕ, which declines only inversely with the radial distance from the star.

Other empirical tests of the theory. The variable extinction of some T Tauri stars (*54*) indicates that dust may be lofted along with the gas of T Tauri winds. The time scale of the variability (hours to days) points to an origin within a few stellar radii of the central star. The ultimate astronomical test may come within the next decade, when a new generation of infrared interferometers (*55*) may allow the direct imaging of the innermost regions of magnetically truncated disks in young stellar objects and their associated dust-laden x-winds and funnel flows.

The richest confrontations between theory and data, however, may still come from the chondritic meteorites. For future studies, we recommend that detailed comparisons of the computed thermal histories of CAIs and chondrules be made with (i) the petrological data on chondrule and CAI textures (*8*, *9*) and (ii) the evidence for evaporation and gas exchange in CAIs and chondrules, for example, mass fractionations that favor heavier isotopes and especially the oxygen data on chondrule suites (*56*). The chondritic meteorites indisputably contain important information concerning the history of the early solar system. We now need to ascertain which pieces of evidence pertain to the conditions at 0.06 AU and which pertain to the conditions at 2.5 AU and larger.

REFERENCES

1. D. W. G. Sears and R. T. Dodd, in *Meteorites and the Early Solar System*, J. F. Kerridge and M. S. Matthews, Eds. (Univ. of Arizona Press, Tucson, 1988), pp. 3–31.
2. A. G. W. Cameron, *Icarus* **92**, 204 (1962); *Annu. Rev. Astron. Astrophys.* **26**, 441 (1988); V. S. Safranov, *Evolution of the Protoplanetary Cloud and Formation of the Earth and Planets* (Nauka, Moscow, 1969; NASA-TT-F-677, 1972); C. Hayashi, *Prog. Theor. Phys.* **70**, 35 (1981); G. W. Wetherill, *Annu. Rev. Earth Planet. Sci.* **18**, 205 (1990); J. Lissauer, *Annu. Rev. Astron. Astrophys.* **31**, 129 (1993).
3. S. J. Weidenschilling and J. N. Cuzzi, in *Protostars and Planets III*, E. H. Levy and J. I. Lunine, Eds. (Univ. of Arizona Press, Tucson, 1993), pp. 1031–1060.
4. S. R. Taylor, *Solar System Evolution* (Cambridge Univ. Press, Cambridge, 1992).
5. F. H. Shu, F. C. Adams, S. Lizano, *Annu. Rev. Astron. Astrophys.* **25**, 23 (1987); K. M. Strom, S. E. Strom, S. E. Edwards, S. Cabrit, M. F. Skrutskie, *Astron. J.* **97**, 1451 (1989); S. V. W. Beckwith and A. I. Sargent, in (*3*), pp. 521–542; C. Bertout, *Annu. Rev. Astron. Astrophys.* **27**, 351 (1989).
6. E. H. Levy, in (*1*), pp. 697–711; J. F. Kerridge, *Icarus* **106**, 135 (1993); E. A. King, Ed., *Chondrules and Their Origins* (Lunar and Planetary Institute, Houston, TX, 1983).
7. J. Wisdom, *Icarus* **56**, 51 (1983); *Nature* **315**, 731 (1985); G. W. Wetherill, *Meteoritics* **20**, 1 (1985).
8. R. H. Hewins, in (*1*), pp. 660–679.
9. G. J. MacPherson, D. A. Wark, J. T. Armstrong, in (*1*), pp. 746–807.
10. D. N. C. Lin and J. Papaloizou, in (*45*), pp. 981–1072; *Annu. Rev. Astron. Astrophys.* **33**, 481 (1995); P. Bodenheimer, *ibid.*, p. 199; P. Cassen and A. P. Boss, in (*1*), pp. 304–328.
11. S. V. W. Beckwith, A. I. Sargent, R. S. Chini, R. Gusten, *Astron. J.* **99**, 924 (1990); O. P. Lay, J. E. Carlstrom, R. E. Hills, J. G. Phillips, *Astrophys. J.* **434**, L75 (1994); C. J. Chandler, D. W. Koerner, A. I. Sargent, D. O. S. Wood, *ibid.* **449**, L139 (1995); D. W. Koerner, C. J. Chandler, A. I. Sargent, *ibid.* **452**, L69 (1995); L. G. Mundy *et al.*, *ibid.*, in preparation.
12. J. A. Wood, in *Chondrules and the Protoplanetary Disk* (LPI Contrib. 844, Lunar and Planetary Institute, Houston, TX, 1994), pp. 45–46.
13. G. H. Herbig, *Astrophys. J.* **217**, 693 (1977); W. R. Skinner, *Lunar Planet. Sci.* **XXI**, 1166 (1990); K. Liffman, *Icarus* **100**, 608 (1992); _____ and M. Brown, *ibid.* **116**, 275 (1995); in *Chondrules and the Protoplanetary Disk*, in press; G. R. Huss, *Earth Moon Planets* **40**, 165 (1988).
14. A. G. W. Cameron, *Meteoritics* **30**, 133 (1995).
15. C. J. Lada and F. H. Shu, *Science* **248**, 564 (1990).
16. F. Shu *et al.*, *Astrophys. J.* **429**, 781 (1994).
17. F. Shu, J. Najita, S. Ruden, S. Lizano, *ibid.*, p. 797; F. Shu, J. Najita, E. Ostriker, H. Shang, *ibid.*, in press.
18. J. R. Najita and F. H. Shu, *ibid.* **429**, 808 (1994).
19. E. Ostriker and F. H. Shu, *ibid.* **447**, 813 (1995).
20. P. Ghosh and F. K. Lamb, *ibid.* **223**, L83 (1978); A. Königl, *ibid.* **370**, L39 (1991).
21. S. Edwards *et al.*, *Astron. J.* **106**, 372 (1993).
22. F. C. Adams and F. H. Shu, *Astrophys. J.* **308**, 836 (1986).
23. S. W. Stahler, *ibid.* **332**, 804 (1988).
24. J. T. Wasson, *Meteorites—Their Record of the Early Solar System* (Freeman, New York, 1985).
25. H. Palme, J. W. Larimer, M. E. Lipshutz, in (*1*), pp. 436–461.
26. J. N. Grossman, in (*1*), pp. 680–696.
27. E. L. Wright, *Astrophys. J.* **320**, 818 (1987); P. Meakin and B. Donn, *ibid.* **329**, L39 (1988); S. J. Weidenschilling, *Icarus* **60**, 553 (1984); D. C. Richardson, *ibid.* **115**, 320 (1995).
28. W. V. Boynton and D. A. Wark, *Lunar Planet. Sci.* **XVIII**, 117 (1987).
29. S. Chandrasekhar, *Proc. R. Soc. London Ser. A* **286**, 1 (1965).
30. S. J. Weidenschilling, B. Donn, P. Meakin, in *The Formation and Evolution of Planetary Systems*, H. Weaver, F. Paresce, L. Danley, Eds. (Cambridge Univ. Press, Cambridge, 1989), pp. 131–150; D. E. Brownlee, *Annu. Rev. Earth Planet. Sci.* **13**, 147 (1985).
31. S. J. Weidenschilling, *Icarus* **44**, 172 (1980).
32. G. E. Archie, *Trans. Am. Inst. Min. Metall. Pet. Eng.* **146**, 64 (1945); M. Sahimi, *Rev. Mod. Phys.* **65**, 1393 (1993).
33. L. D. Landau and E. Lifshitz, *Statistical Physics* (Pergamon, New York, 1980), part 1, p. 255.
34. H. Nagahara, in (*12*), pp. 25–26.
35. J. N. Grossman, A. E. Rubin, H. Nagahara, E. A. King, in (*1*), pp. 619–659.
36. J. T. Wasson, in *Chondrules and the Protoplanetary Disk*, in press.
37. A. G. G. M. Tielens, C. F. McKee, C. G. Seab, D. J. Hollenbach, *Astrophys. J.* **431**, 321 (1994).
38. J. N. Cuzzi, A. Dobrovolskis, R. C. Hogan, in (*12*), pp. 6–7.
39. P. G. Martin and C. Rodgers, *Astrophys. J.* **322**, 374 (1987); M. Jura, *ibid.* **434**, 713 (1994).
40. E. R. D. Scott, S. G. Love, I. D. Hutcheon, in (*12*), pp. 36–37.
41. G. E. Lofgren, in (*12*), pp. 19–20.
42. A. Tsuchiyama, H. Nagahara, T. Kushiro, *Geochim. Cosmochim. Acta* **45**, 1357 (1981); Y. Yu, R. H. Hewins, H. C. Connolly, in (*12*), pp. 46–47.
43. A. E. Rubin, B. Fegley, R. Brett, in (*1*), pp. 488–511; B. Fegley and H. Palme, *Earth Planet. Sci. Lett.* **72**, 311 (1985).
44. S. E. Edwards, T. Ray, R. Mundt, in (*3*), pp. 567–602.

45. C. Hayashi, K. Nakazawa, Y. Nakagawa, in *Protostars and Planets II*, D. C. Black and M. S. Matthews, Eds. (Univ. of Arizona Press, Tucson, 1985), pp. 1100–1154.
46. E. R. D. Scott, D. J. Barber, C. M. Alexander, R. Hutchison, J. A. Peck, in (*1*), pp. 718–745; B. Donn, *Astron. Astrophys.* **235**, 441 (1990).
47. H. Palme, in (*12*), p. 30.
48. J. W. Larimer and J. T. Wasson, in (*1*), pp. 394–435.
49. H. Palme and W. V. Boynton, in (*3*), pp. 979–1004.
50. I. D. Hutcheon, G. R. Huss, G. J. Wasserburg, *Lunar Planet. Sci.* **XXV**, 587 (1994); I. D. Hutcheon and R. H. Jones, *ibid.* **XXVI**, 647 (1995); G. J. MacPherson *et al.*, *Meteoritics* **30**, 365 (1995).
51. T. Lee, D. A. Papanastassiou, G. J. Wasserburg, *Geophys. Res. Lett.* **3**, 109 (1976); *Astrophys. J.* **211**, L107 (1977).
52. T. Lee, *Astrophys. J.* **224**, 217 (1978); D. D. Clayton and L. Jin, *ibid.* **451**, L87 (1995).
53. N. Sugiura and D. W. Strangeway, in (*1*), pp. 595–615.
54. A. H. Joy, *Astrophys. J.* **102**, 168 (1945); J. G. Bellingham and G. S. Rossano, *Astron. J.* **85**, 555 (1980); J. A. Graham, *Publ. Astron. Soc. Pac.* **104**, 479 (1989); N. L. Eaton and W. Herbst, *Astron. J.* **110**, 2369 (1995).
55. J. T. Armstrong, D. J. Hutter, K. J. Johnston, D. Mozurkewich, *Phys. Today* **48**, 42 (May 1995).
56. R. N. Clayton, T. K. Mayeda, C. A. Molini-Velsko, in (*45*), pp. 755–771.

31 July 1995; accepted 3 January 1996

A Permease-Oxidase Complex Involved in High-Affinity Iron Uptake in Yeast

Robert Stearman, Daniel S. Yuan, Yuko Yamaguchi-Iwai, Richard D. Klausner, Andrew Dancis*

Iron must cross biological membranes to reach essential intracellular enzymes. Two proteins in the plasma membrane of yeast—a multicopper oxidase, encoded by the *FET3* gene, and a permease, encoded by the *FTR1* gene—were shown to mediate high-affinity iron uptake. *FET3* expression was required for FTR1 protein to be transported to the plasma membrane. *FTR1* expression was required for apo-FET3 protein to be loaded with copper and thus acquire oxidase activity. FTR1 protein also played a direct role in iron transport. Mutations in a conserved sequence motif of FTR1 specifically blocked iron transport.

Cells require iron for a wide array of metabolic functions (*1*, *2*), and yet iron can be toxic when present in excess (*3*). Alterations of iron pools have been implicated in diverse human disease processes, including neurodegenerative diseases (*4*, *5*), aging (*4*), microbial infections, atherosclerosis, and cancer (*6*). In order to acquire iron from the environment, cells must solubilize insoluble ferric iron (*7*), transport the iron across a membrane into the cytosol, and regulate the uptake process to maintain cellular iron concentrations within a tightly controlled range. The molecular details of iron transport in most eukaryotes have remained unsolved (*8*, *9*).

High-affinity iron uptake in the yeast *Saccharomyces cerevisiae* requires copper (*10*, *11*). This copper requirement is explained by the involvement of a copper-containing oxidase, FET3, in iron uptake (*10*, *11*). Because the FET3 oxidase activity is required for iron uptake, copper deficiency or mutations in genes involved in delivery of copper to FET3 abrogate iron uptake as a secondary effect. These genes include *CTR1*, the cellular copper uptake transporter (*10*), and *CCC2*, an intracellular copper transporter (*12*). The human multicopper oxidase ceruloplasmin exhibits similarity to the yeast FET3 oxidase (*11*). Ceruloplasmin plays an important role in human iron homeostasis. Copper deficiency has been associated with apparent iron deficiency because of a lack of ceruloplasmin activity (*13*). The inherited disorder, Wilson disease, also associated with deficient ceruloplasmin activity, results from mutations in the gene for a copper-transporting P-type adenosine triphosphatase (ATPase) (*14*) with strong similarity to the *CCC2* gene product in yeast (*15*). Severely affected individuals with Wilson disease may exhibit abnormalities of iron transport (*16*). Recently, mutations in the ceruloplasmin gene itself have been identified as the cause of a neurodegenerative syndrome characterized by the failure to export iron from various tissues, including the basal ganglia in the brain (*5*). One interpretation of these findings is that multicopper oxidases (FET3 in yeast, or ceruloplasmin in humans) are required for iron transport across membranes (*17*), although the precise role of such oxidases in mediating iron transport remains unclear. FET3 has a single hydrophobic domain and is localized to the plasma membrane (*18*). Its protein sequence bears no resemblance to that of the family of permeases, and thus it has been difficult to understand how FET3 by itself could mediate iron transport.

We describe another component of the iron uptake system in yeast that fulfills expectations for an iron transporter in having multiple predicted transmembrane domains and iron-binding motifs. Expression is homeostatically regulated through the action of the AFT1 regulatory protein (*19*), as predicted for an element of the iron uptake system and similar to the regulation of FET3 (*11*, *19*). This component appears to work in concert with the FET3 multicopper oxidase to mediate the transmembrane transport of iron into the cell.

FTR1, a candidate gene for the iron transporter. A method for selecting mutants in iron uptake (*10*) or iron sensing (*19*) was devised with the iron-regulated promoter of the *FRE1* gene. Transcription of the *FRE1* gene is repressed in cells grown in the presence of iron (*20*). The *FRE1* promoter was fused to the coding region of the *HIS3* gene and integrated into a haploid yeast strain carrying a deletion at the *HIS3* locus. In this engineered strain, expression of the *HIS3* gene product driven by the *FRE1* promoter was repressed by addition of iron to the growth medium. Spontaneous mutants appeared and grew into colonies on media with high iron and no histidine. Strain E31 (*21*, *22*), which grew under the selective conditions, completely lacked high-affinity iron uptake and was analyzed further. When mutant haploid strains derived from E31 were crossed with strains mutated at the *CTR1*, *CCC2*, or *FET3* loci, the diploids generated by these crosses exhibited normal levels of iron uptake. Thus, E31 contained a recessive mutation in a previously uncharacterized gene required for iron uptake, which we called *FTR1* (for Fe transporter) (*22*).

Evaluation of *FTR1* mutants revealed phenotypic similarity to *FET3* mutants. High-affinity iron uptake was absent (Fig. 1), and manipulation of the copper concentration of the growth medium did not correct this deficiency, even when copper was added at concentrations capable of correcting the defect in a *CCC2* mutant (Fig. 1). Growth and colony formation were unimpaired in rich medium or defined medium with sufficient iron (*23*). However, under conditions of iron deprivation created by the iron chelator ferrozine (*24*), growth of the *ftr1-1* mutant and the *fet3-2C* mutant were similarly inhibited (*23*).

To isolate the *FTR1* gene, we trans-

Cell Biology and Metabolism Branch, National Institutes of Child Health and Human Development, National Institutes of Health, Bethesda, MD 20892, USA.

*To whom correspondence should be addressed.